NUKLEONIKA 2012;57(2):283–286

ORIGINAL PAPER

Laser ablated carbon plume: experiment and modelling

Tomasz Moscicki,
Jacek Hoffman,
Zygmunt Szymanski

Abstract. Laser ablation of graphite is studied both theoretically and experimentally. Plasma temperature and electron density in the early phase of expansion into vacuum are measured as a function of distance from the target. The experimental results agree well with the theoretical simulations. The simulation of ablation shows that plasma plume considerably affects the ablation rate.

Key words: laser ablation • plasma plume

T. Moscicki✉, J. Hoffman, Z. Szymanski
Institute of Fundamental Technological Research,
5B Pawińskiego Str., 02-106 Warsaw, Poland,
Tel.: +48 22 826 1281, Fax: +48 22 826 7380,
E-mail: tmosc@ippt.gov.pl

Received: 21 September 2011
Accepted: 28 November 2011

Introduction

Laser ablation is a well-established method of removing material from a solid surface by irradiating it with a laser beam. During laser ablation, the material evaporated from the target forms a thin layer of very dense gas, consisting of electrons, ions and neutrals. This plasma plume absorbs energy from the laser beam, and its temperature and pressure grow [9]. The ablation rate is strongly affected by the plasma formation because the dense plasma plume can entirely block laser radiation and subsequently energy transfer from the laser beam to the material [2, 9].

In this paper, the ablation of graphite is studied both theoretically and experimentally. Theoretical modelling of the target heating and plasma formation during interaction with the nanosecond laser pulse is presented and compared with the experiment. Graphite was chosen because its ablation is used to obtain a wide variety of carbon-containing materials, such as diamond-like carbon [14], fullerene carbon molecules [4] and carbon nanotubes [11], as well as for the removal of co-deposited layers from plasma limiters in tokamaks [13].

Theoretical model

The model [10] which describes both the target heating, formation of the plasma and its expansion consists

of equations of conservation of mass, momentum and energy and is solved in axial symmetry with the use of the Fluent software package [1]. In the case of a nanosecond laser, the ablation is thermal and hence the initial conditions for plume expansion were taken from the theory of the rapid surface vaporization [5]. It has been assumed that the vapour velocity at the end of the Knudsen layer is sonic and the other parameters are $T_v \sim 0.67\ T_s$, $p_v \sim 0.21\ p_s$, $\rho_v \sim 0.31\ \rho_s$ where the subscript s denotes the surface [5]. The temperature T_s is determined by solving the heat transfer equation and the pressure p_s is calculated from the Clausius--Clapeyron equation [5].

The target heating is described by the equation

$$\frac{\partial(\rho H)}{\partial t} + div(\rho \vec{u} H) = div(k \nabla T) + (1-R)\cdot\alpha\cdot I_S \cdot \exp(-\alpha z) \tag{1}$$

where H is enthalpy $H = \int_{T_0}^{T} c_p\, dT + L_m$,

c_p is the specific heat at constant pressure, L_m is the latent heat of melting, ρ is the mass density of the target material, k is the thermal conductivity, T is the temperature, R is the target reflectivity, α is the graphite absorption coefficient, $I_S = I_L \cdot \exp(-\int \kappa dz)$ where I_L is the laser intensity, κ is the plasma absorption coefficient, z is the axial coordinate and $\vec{u}$ is the recession velocity given by the Hertz-Knudsen equation,

$$u(t) = (1-\beta)\frac{p_s}{\rho}\left(\frac{m}{2\pi k T_s}\right)^{1/2} \tag{2}$$

where β is the fraction of the vaporized particles returning to the target surface (back flux) and m is the particle mass. The energy source term I_L was used in the form which fits the shape of the laser pulse.

The boundary condition at the place where the laser beam strikes the surface is

$$-k\frac{\partial T_s}{\partial \vec{n}} = -\rho u(t) L_v \tag{3}$$

where L_v is the latent heat of vaporization and $\vec{n}$ is the unit vector perpendicular to the surface.

During the first few hundreds of nanoseconds after beginning of the laser pulse the plasma is so dense, that it can be treated as continuum fluid and equations of gasdynamics can be applied for its description. The set of equations consists of equation of conservation of mass, energy, momentum and a convection-diffusion equation in the form [1, 10]:

$$\frac{\partial \rho}{\partial t} + \nabla\cdot(\rho\vec{v}) = 0 \tag{4}$$

$$\frac{\partial}{\partial t}(\rho E) + \nabla\cdot(\vec{v}(\rho E + p)) = \kappa\cdot I_z - \Re \tag{5}$$

$$\frac{\partial}{\partial t}(\rho\vec{v}) + \nabla\cdot(\rho\vec{v}\vec{v}) = -\nabla p + \rho\vec{g} \tag{6}$$

$$\frac{\partial}{\partial t}(\rho Y_i) + \nabla\cdot(\rho\vec{v}Y_i) = 0 \tag{7}$$

where E is energy $E = H - p/\rho + 0.5v^2$, I_z is the local laser intensity, p is the pressure, $\vec{v}$ is the velocity vector, $\Re$ is the radiation loss function, and $\vec{g}$ is the gravity, Y_i is the mass fraction of ablated vapour in the mixture with residual air. In the first phase of the plume expansion, the gasdynamic effects prevail over the transport phenomena and the momentum equation can be used in the Euler form. The mass density and the specific heat of carbon vapour were calculated in all necessary ranges of pressure, assuming the local thermodynamic equilibrium. At $z = 0$, $r < r_L$, where r_L is the radius of the laser beam the conditions at the end of the Knudsen layer were assumed. Details of modelling can be found in [10].

Experiment

Graphite target irradiation was performed using a Nd:YAG laser operating at its fundamental wavelength of 1064 nm with pulse energy of ~ 400 mJ and 10 ns pulse duration. The laser spot on the target was 2.5 mm^2, which resulted in the laser fluence of ~ 15 J·cm^{-2} (intensity, I = 1.5 GW·cm^{-2}). The incident angle of the laser beam was 45° to the surface normal. A pyrolytic graphite target from Kurt J. Lesker was used (density 2.18×10^3 kg·m^{-3}, purity 99.999%). The target was rotated to avoid crater formation. The ablated plume expanded in a chamber evacuated to a background pressure of 1×10^{-4} Pa. The experimental setup was similar to that described in [3]. The emission spectra of the plasma plume was registered with the use of a spectrograph/monochromator (Acton, model SpectraPro2500i) and an ICCD camera. The spectrograph was equipped with three gratings 2400, 1800, and 600 grooves/mm. In the case of 2400 g/mm, the reciprocal dispersion in the visible region was 0.005÷0.008 nm/pixel depending on wavelength. The width of the entrance slit was 50 μm. The plasma was imaged on the entrance slit using a 300 mm achromatic lens mounted on a movable table. The magnification was 1. The camera was gated by a digital delay generator triggered by the signal from the laser. The exposure time (gate width) was 10 ns. The delay time changed from 15 ns to 180 ns.

The emission spectra consisted of C IV, C III and C II ions lines. The atomic lines were not observed in the delay times studied. The electron densities were determined from the Stark broadening of the C IV 580.13 nm, C III 569.59 nm and 464.74 nm lines and at greater distances from the Stark broadening of the C II 426.70/72, 566.24 and 657.80 nm lines. The Stark broadening parameters were taken from [6, 7]. The apparatus half-width was measured with the use of a low pressure spectral lamp. Close to the target, the electron temperature was determined from the ratio of intensities of the C IV 580.13 nm and C III 569.59 nm lines (multiplied by the electron density). Farther from the relative intensities of the C III 466.58, 466.36, 467.39, 464.74, 465.02, 465.14, and 569.59 nm lines (Boltzmann plot) and from the ratio of intensities of the C III 569.59 nm and C II 566.24 nm lines. The transition probabilities were taken from [12] and [8]. The lines used for determination of the electron density, and temperature were checked to be free from self-absorption according to the method described in [3].

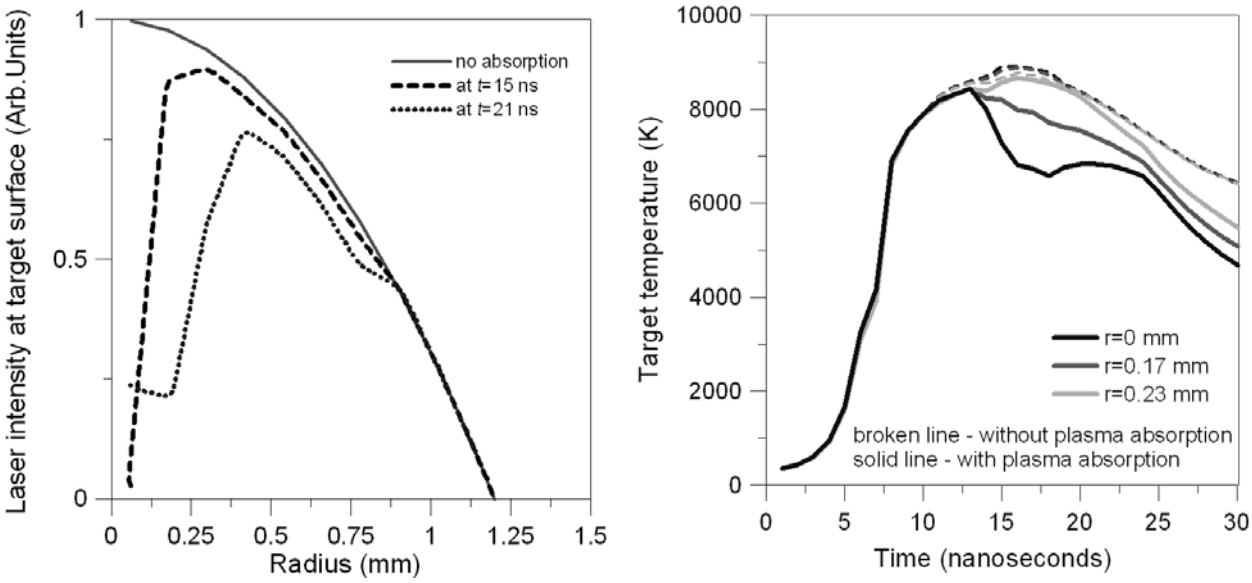

Fig. 1. Laser intensity and target temperature at various moments of the laser pulse.

Results

The effect of plasma absorption on the laser intensity distribution and the target surface temperature is shown in Fig. 1. The temperature of the target surface reaches a maximum of 8400 K at the axis centre at $t = 13$ ns after the beginning of the laser pulse. At the same moment, plasma plume forms ahead of the target and then laser intensity at the axis practically drops to zero within a few nanoseconds. The plasma absorption is the strongest in the centre of the laser beam and consequently, the temperature of the target is affected mainly at small radii.

The observed changes of the temperature of the target surface, due to plasma absorption results in the decrease of total ablation rate of ~ 15% in comparison to the unaffected laser beam. The calculated amount of ablated matter – 0.81 μg·mm^{-2}·pulse^{-1} is close to that obtained experimentally – 0.84 μg·mm^{-2}·pulse^{-1} at the fluence 15 J·cm^{-2}. The experimental value was obtained by measuring the target weight before and after 3000 shots.

Figure 2 shows the distributions of the plasma temperature and electron density 40 ns from the beginning of the laser pulse. The development of the plasma results in the growth of temperature and consequently, the increase of pressure which in turn accelerates the plume. The plasma flow velocity increases from the initial 3×10^3 m·s^{-1} to 6×10^4 m·s^{-1}.

The experimental and theoretical results are compared in Fig. 3 where the axial electron temperatures and densities at two different delay times are presented as a function of a distance from the target. The agreement between the experiment and the theoretical model is fairly good at delay times greater than 60 ns.

Summary

The simulated profiles of the plasma temperature and electron density in the early phase of expansion are in reasonable agreement with the experimental profiles obtained from the emission spectroscopy. This shows that the hydrodynamic model applied fairly well de-

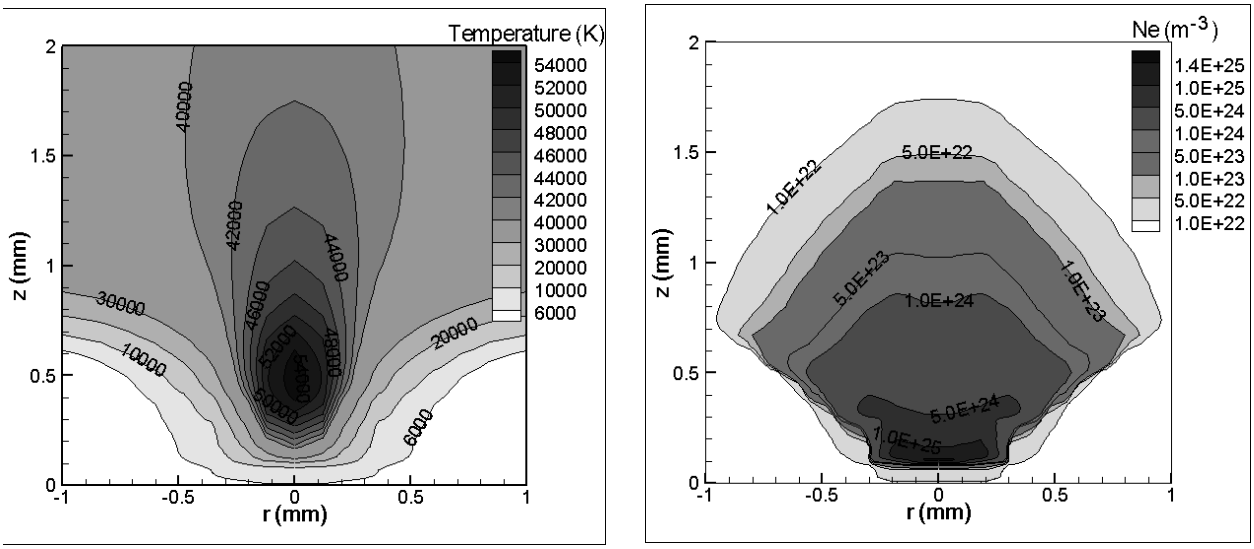

Fig. 2. Distribution of the plasma temperature and electron density 40 ns from the beginning of the laser pulse.

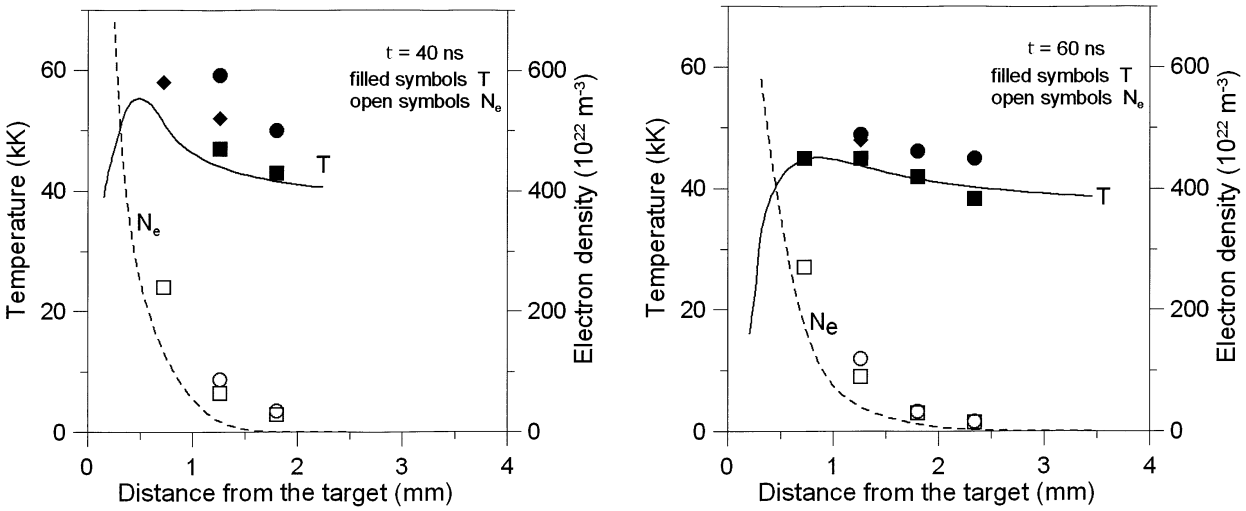

Fig. 3. Axial electron temperature and density as a function of a distance from the target. Delay time t = 40 and 60 ns. Symbols – experiment; ◆ from the ratio of intensities C IV 580.13/C III 560.59 nm lines; ● from relative intensities of C III lines; ■ from the ratio of intensities C III 569.59/C II 566.24 nm lines. Lines – theoretical model.

scribes an evolution of the plasma plume. The results of the calculations show that the plasma induced during the laser ablation has a significant effect on the ablation rate. At laser fluence $F = 15$ J·cm^{-2} the ablation rate is ~ 15% lower in comparison to the unaffected laser beam.

Acknowledgment. This work was supported by the Research Project N N501 069138.

References

1. FLUENT 6.3. User's Guide
2. Harilal SS, Sizyuk T, Hassanein A, Campos D, Hough P, Sizyuk V (2011) The effect of excitation wavelength on dynamics of laser-produced tin plasma. J Appl Phys 109:063306
3. Hoffman J, Mroz W, Prokopiuk A, Szymanski Z (2008) Plasma plume induced during laser ablation of graphite. Appl Phys A: Mater Sci Process 92:921–926
4. Hunter J, Fye J, Jarrold MF (1993) Annealing C60+: Synthesis of fullerenes and large carbon rings. Science 260:784T–786T
5. Knight CJ (1979) Theoretical modeling of rapid surface vaporization with back pressure. AIAA J 17:519–523
6. Konjevic N, Lesage A, Wiese WL (2002) Experimental Stark widths and shifts for spectral lines of neutral and ionized atoms (A critical review of selected data for the period 1989 through 2000). J Phys Chem Ref Data 31:819–927
7. Konjevic N, Wiese WL (1990) Experimental Stark widths and shifts for spectral lines of neutral and ionized atoms. J Phys Chem Ref Data 19:1307–1385
8. Kurucz RL, Bell B (1995) Atomic Line Data, Kurucz CD-ROM No. 23. Smithsonian Astrophysical Observatory, Cambridge
9. Mazhukin VI, Nossov VV, Smurov I (2007) Modeling of plasma-controlled evaporation and surface condensation of Al induced by 1.06 and 0.248 μm laser radiations. J Appl Phys 101:024922
10. Moscicki T, Hoffman J, Szymanski Z (2011) Modelling of plasma formation during nanosecond laser ablation. Arch Mech 63:99–116
11. Puretzky A, Schittenhelm H, Fan X, Lance MJ, Allard Jr FL, Geohegan DB (2002) Investigations of single-wall carbon nanotube growth by time-restricted laser vaporization. Phys Rev B 65:245425
12. Ralchenko Yu, Kramida AE, Reader J (2010) NIST Atomic Spectra Database (ver. 4.0.0). NIST ASD Team, National Institute of Standards and Technology, Gaithersburg
13. Wolowski J, Gasior P, Hoffman J, Kubkowska M, Rosinski M, Szymanski Z (2010) Study of laser-induced removal of co-deposits from tokamak plasma-facing components using ion diagnostics and optical spectroscopy. Radiat Eff Defects Solids 165:434–440
14. Yoshitake T, Nishiyama T, Aoki H, Suizu K, Takahashi K, Nagayama K (1999) The effects of substrate temperature and laser wavelength on the formation of carbon thin films by pulsed laser deposition. Diamond and Related Materials 8:463–467